Journal of Materials Chemistry C

PAPER

View Article Online
View Journal | View Issue

Cite this: J. Mater. Chem. C, 2018, 6, 9517

High pump efficiency of a second-order distributed feedback laser based on holographic polymer dispersed liquid crystals with preferred liquid crystal molecular orientation

Lijuan Liu, *[a] Xiaobo Kong,[a] Qidong Wang,[b] Yonggang Liu[b] and Li Xuan[b]

Received 11th July 2018,
Accepted 8th August 2018

DOI: 10.1039/c8tc03412e

rsc.li/materials-c

We report on the fabrication and characterization of a surface-emitting distributed feedback (DFB) organic semiconductor laser based on a holographic polymer dispersed liquid crystal (HPDLC) transmission grating. Specifically, by adopting an acrylate-based monomer with low functionality and a narrower grating, the phase separated liquid crystal (LC) molecules were aligned along the direction of the grating groove, which can exhibit better lasing feedback performance in the HPDLC layer. The device shows single-mode laser emission at 630.4 nm with a threshold of 0.18 μJ, and the conversion efficiency is 6.4%. The curing intensity, light loss and diffraction efficiency were also investigated for HPDLC structures to identify the effects of the grating period and monomer functionality.

1. Introduction

Organic semiconductor lasers (OSLs) have attracted considerable scientific interest because of their potential for use as optical sources in high sensitivity spectroscopy,[1] sensors for explosive vapors[2] and ultrafast switches in all-optical data communication.[3] Organic semiconducting materials possess the combined optical and electronic properties of organic gain media and semiconductors, showing advantages such as low cost, strong absorption, simple process and wide absorption bands. Compared with organic dyes, organic semiconducting materials have small concentration quenching, thus OSLs could allow optical pumping by light-emitting diodes[4] or inorganic laser diodes,[5] which is promising for compact laser applications. OSLs have already been demonstrated in a variety of resonator structures, such as Fabry–Pérot, microcavities, microrings, microspheres and distributed feedback (DFB). DFB structures have desired resonator geometries due to low thresholds and single longitudinal mode emission as a result of their long gain path and high wavelength selectivity.[6] So far, many DFB OSLs have been prepared *via* electron beam lithography,[7] hot embossing technique,[8] UV nanoimprint lithography[9] and interference ablation technique.[10] In these OSLs, the active layer acts as both the gain layer and the index modulation layer, which makes the coupling mechanism complex. A HPDLC transmission grating is used as the DFB configuration cavity because of its ease of preparation[11] and has low optical scattering[12] and electrical tunability.[13] A HPDLC grating contains alternating polymer-rich and LC-rich lamellae, which is prepared in a single-step exposure of a homogeneous mixture of prepolymer/LC mixture to an interference fringe pattern by the photo-polymerization induced phase separation (PIPS) method. The average orientation of liquid crystal molecules in HPDLCs is perpendicular to their holographic planes with Raman spectroscopy,[11] and the orientation is ascribed to the anchoring energy of polymer fibers between adjacent polymer planes.[14] Thus for feedback lights propagating along the grating vector, the effective light feedback output is not high. Previously, we have presented a high feedback laser by adopting a low functional monomer to lower the surface anchoring of the polymer fibers and using a rubbed PI alignment layer.[15] The threshold was decreased to 0.25 μJ (*i.e.*, pump energy density of 0.05 mJ cm^{-2} or perk power density per pump laser pulse of 6.25 kW cm^{-2}, the same as below) and the conversion efficiency was increased to 4.6%.

In this work, we report on a second-order DFB OSL using a HPDLC as the external feedback layer. The phase separated LCs were aligned along the direction of the grating groove with no rubbed PI alignment layer. In addition to all the advantages of the previous study,[15] this DFB laser shows surface-emitting laser emission with a lower threshold of 0.18 μJ and a higher conversion efficiency of 6.5%. We found that there was another anchoring energy generated from grating grooves competing with the surface anchoring of the polymer fibers, and the anchoring energy is dominant in samples with small periods.

[a] School of Physics and Physical Engineering, Shandong Provincial Key Laboratory of Laser Polarization and Information Technology, Qufu Normal University, 273165, Qufu, China. E-mail: llj2007weihai@163.com
[b] State Key Laboratory of Applied Optics, Changchun Institute of Optics, Fine Mechanics and Physics, Chinese Academy of Sciences, Changchun, 130033, China

The phase separated LCs are along the direction of the grating groove, therefore the refractive index difference in the HPDLC feedback layer can be increased and the lasing performance can be enhanced.

2. Device fabrication

The device structure is illustrated in Fig. 1a. The solution of MEH-PPV (average molecular weight of 120 000, OLED Material Tech.) in chlorobenzene (CB) solvent (8 mg ml^{-1}) was deposited onto the bottom glass substrate by spin-coating (2000 rpm; 30 s), resulting in a homogeneous thin film. After spin-coating, the MEH-PPV film was heated in a vacuum oven at a 2 °C min^{-1} heating rate from room temperature to 120 °C and kept at 120 °C for 1 h, and then slowly cooled to room temperature. A smoother surface was observed, as shown in Fig. 1b. The MEH-PPV layer with a thickness of ~80 nm was measured using a Dektak profilometer, and the photoluminescence quantum yield (PLQY) value was increased from 23% to 32%.[16] By combining the MEH-PPV coated glass substrate with a bare glass substrate, an empty cell was formed. The cell gap was controlled at 6 μm by using Mylar spacers. To form the HPDLC pre-polymer syrup, nematic LC TEB30A (n_e = 1.692, Slichem, 28 wt%), monomer (60 wt%), chain extender *N*-vinylpyrrolidone (NVP, Sigma-Aldrich, 10 wt%), co-initiator *N*-phenylglycine (NPG, Sigma-Aldrich, 1.5 wt%), and photo-initiator Rose Bengal (RB, Sigma-Aldrich, 0.5 wt%) were mixed. Different from previous reports,[17,18] only low functional monomer phthalic diglycol diacrylate (PDDA, Sigma-Aldrich) was adopted. The chemical structure of PDDA is shown in Fig. 1c.

The syrup was then injected into the cell by capillary action and put into the holographic optical field to form the HPDLCs. The cell underwent holographic photo-curing by two coherent frequency-doubled, 532 nm continuous Nd-YAG laser beams for 5 min. The grating period (Λ) can be calculated and controlled according to $\Lambda = \frac{\lambda_{532}}{2\sin(\theta/2)}$, and θ was the intersection angle of the two coherent recording beams. The period of the gratings was chosen to be 395 nm in this work. The grating shows a scaffolding-like morphology, in which the phase-separated LCs exist in the form of pure slices instead of droplets.[18] To characterize the properties of HPDLCs, diffraction efficiency and light loss were measured by two He–Ne lasers (circular polarization, 632.8 nm) at the incident Bragg angle and the normal direction onto the sample, respectively, as described earlier.[12]

The diffraction efficiency is defined as the diffracted light intensity in the first order divided by the incident light intensity, and it includes p light diffraction efficiency (η_p) and s light diffraction efficiency (η_s) here. Fig. 2a shows diffraction efficiency as a function of curing intensity of the sample with a grating period at 395 nm. A curing intensity of 6 mW cm^{-2} gives the best grating, and the highest diffraction efficiency is about 45%. Furthermore, to understand the optimal curing conditions better, the optimum curing intensity for different periods of gratings was also investigated. As shown in Fig. 2b, a narrower grating requires a stronger curing intensity. There are mainly two reasons: firstly, a narrower grating needs a larger intersecting angle θ, which would bring the degradation of the fringe pattern contrast; secondly, the period of grating would influence the formation dynamics, as narrow periods provide little time for diffusion. We will discuss this more in Section 3.1.

3. Device performance

The schematic setup of the lasing experiment is shown in Fig. 3. The holographically cured sample with a grating period at 395 nm was photo-pumped at 532 nm by a Q-switched frequency-doubled

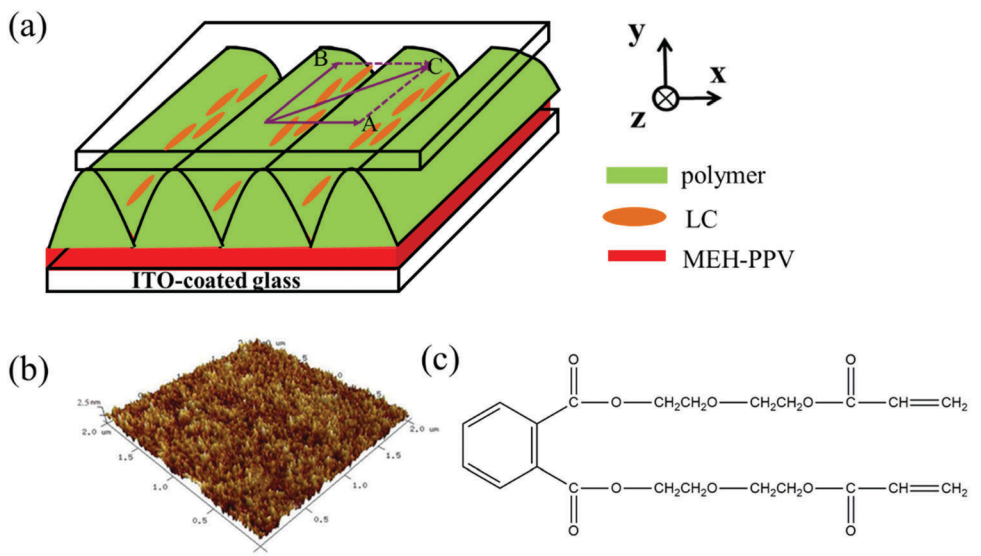

Fig. 1 (a) Schematic structure of the proposed DFB laser configuration with a grating period at 395 nm, (b) the AFM image of the MEH-PPV surface, and (c) the chemical structure of PDDA.

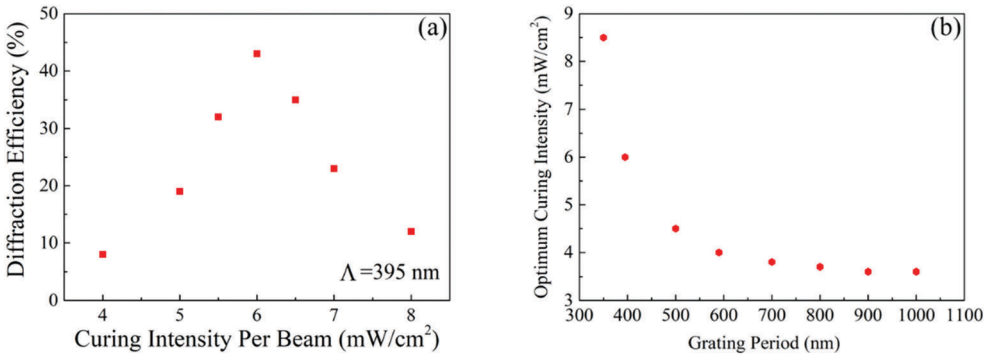

Fig. 2 (a) Diffraction efficiency as a function of curing intensity of the sample and (b) dependence of optimum curing intensity on the grating period.

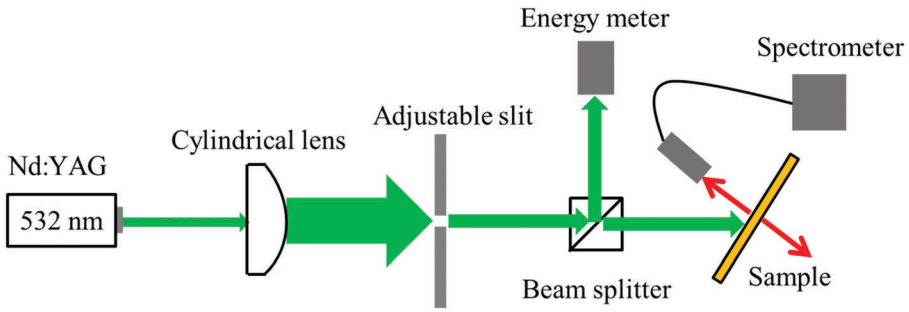

Fig. 3 Optical setup for pumping the organic DFB sample and collecting the output lasing.

Nd:YAG laser (laser wavelength: 532 nm; pulse duration: 8 ns; repetition rate: 1 Hz). A cylindrical lens with a focal length of 20 cm and an adjustable slit were used to shape the pump beam into a narrow stripe (5 mm by 0.1 mm). Then the narrow stripe was divided into two beams with equal intensities by a beam splitter. One beam was used to pump the sample at an angle of 45° with respect to the glass substrate, and the other beam was directed into a pulse energy meter. The output lasing was collected and measured using a fiber pigtail detector coupled spectrometer (LabMax-TOP; Coherent Inc.).

3.1 The orientation of LC molecules in HPDLCs

Since the refractive index of a pure polymer n_p (1.525, measured using an Abbe refractometer) is closer to n_o (1.522) rather than n_e (1.692), the change of the diffraction efficiency in the s or p polarization state is mainly related to n_e, *i.e.*, the orientation of the phase-separated LC molecules. Fig. 4a shows the real-time diffraction efficiencies in different polarization states. The diffraction efficiency for s-polarization is 47% greater than that for p-polarization of 3%, which suggests that the orientation of LC molecules is parallel to the direction of the s-polarization state, *i.e.*, the grating groove (*z* axis, Fig. 1a). The scattering loss in different polarization states can also give clues on LC orientation. From Fig. 4b, we can see the scattering loss for p polarization light is about 2%, while that for s polarization is about 6%, which also indicates that the LC orientation in the HPDLCs is along the grating groove. We think that it is caused by another anchoring energy, and it is generated from grating grooves. There is a competitive relationship between the surface anchoring of the polymer filaments (A in Fig. 1a) and the

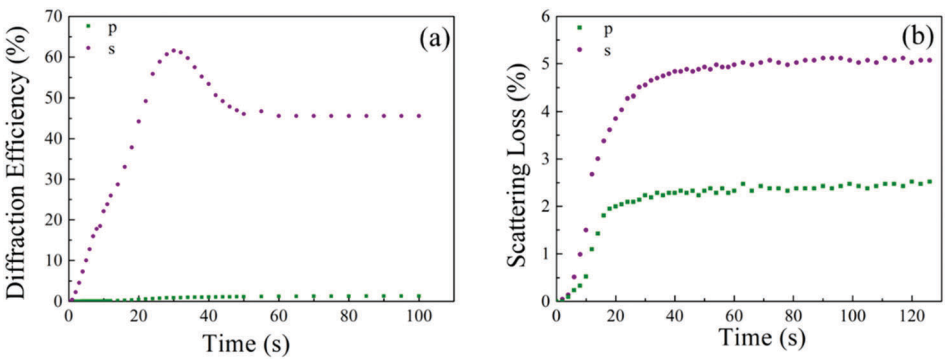

Fig. 4 (a) Real-time diffraction efficiency and (b) light loss for p polarization (square) and s polarization (sphere) for the sample, respectively.

anchoring effect of the grating grooves (B in Fig. 1a). The low functional monomer will produce less polymer filaments in rich-LC regions[19] due to its lower mobility,[20] which exert a smaller anchoring strength on LC molecules than the multi-functional monomer. Thus the anchoring effect of the grating grooves is dominant in the sample. Besides, the scattering loss is much lower than that (>10%) observed in droplet morphologic HPDLC gratings,[21] resulting in the higher conversion efficiency of the pump input to the lasing output.

Furthermore, to study the anchoring effect of the grating grooves in the HPDLCs, the diffraction efficiency and the grating optical sensitivities of the samples with different periods were investigated, as shown in Fig. 5. The diffraction efficiency for p-polarization is obviously greater than that for s-polarization when the grating period is larger than 500 nm (Fig. 5a), and the optical sensitivities become larger as the grating period increases (Fig. 5b). This means that the surface anchoring effect of the polymer filaments is dominant, which makes the majority of phase-separated LCs to be aligned in the grating vector direction. However, the diffraction efficiency for s-polarization is greater than that for p-polarization when the grating period is smaller than 425 nm, thus the anchoring effect of grating grooves is dominant, and the orientation of a majority of LC molecules is parallel to the grating grooves. It is worth noting that there exists a cut-off value of fringe spacing below which no HPDLC gratings can be formed,[22] and the cut-off value is 300 nm in this work.

In HPDLCs, the resultant force (C in Fig. 1a) of surface anchoring of the polymer filaments and the anchoring effect of the grating grooves play a key role in dictating the electro-optical properties. If the resultant force is strong, a larger driving voltage is required to re-orient the LC molecules with the applied field. Fig. 6a shows the diffraction efficiency as a function of the driving electric field for the sample with a grating period at 395 nm. The driving electric field E_{90} is defined as the electric field required for attaining 90% diffraction of the first-order diffraction light out of 100% (without applying electric field). The E_{90} value of the sample is 4.2 V μm^{-1}. The driving electric field E_{90} is presented as a function of grating period as shown in Fig. 6b. It is shown that the smaller the grating period, the larger the driving electric field and the stronger the resultant force. The anchoring energy of polymer fibers in a narrower grating would become weaker,[23] therefore the anchoring energy of grating grooves would become stronger.

3.2 Lasing output

When optically pumped, the laser emission occurred from our device. The lasing wavelength λ_{las} should satisfy the Bragg condition:

$$m\lambda_{las} = 2n_{eff}\Lambda \quad (1)$$

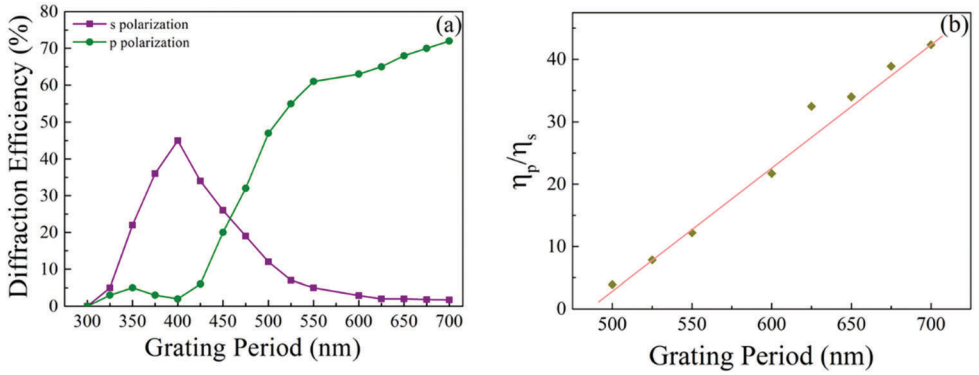

Fig. 5 Dependence of (a) diffraction efficiency for p polarization (sphere) and s polarization (square) and (b) grating optical sensitivities (η_p/η_s) on the grating period.

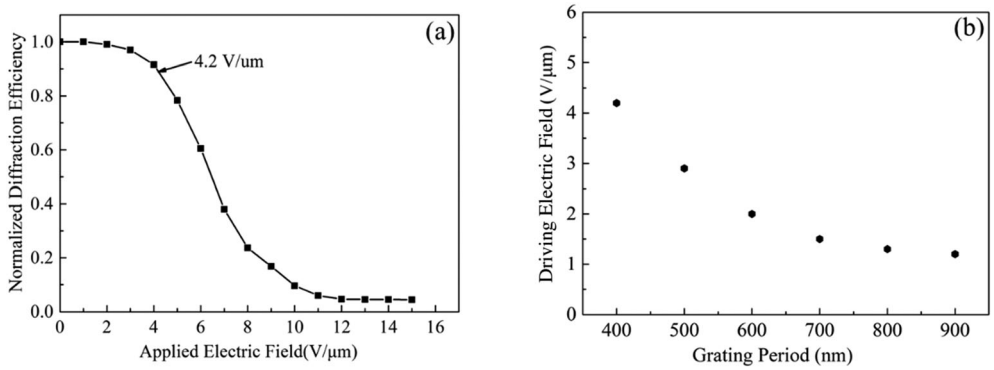

Fig. 6 (a) Diffraction efficiency as a function of the applied electric field for the sample and (b) dependence of the driving electric field E_{90} on the grating period.

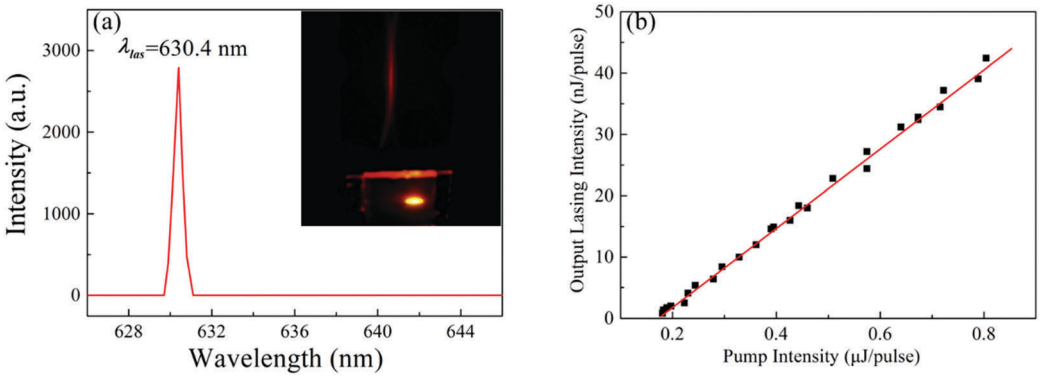

Fig. 7 (a) Output lasing spectrum at 2× threshold, with the inset showing the vertical laser emission on a paper screen and (b) the lasing output intensity as a function of pump intensity for the DFB laser.

where n_{eff} is the effective refractive index of the laser mode and m is the Bragg order, which was selected as 2 in this work. λ_{las} also satisfies the grating coupling equation:

$$\frac{2\pi}{\lambda_{\text{las}}}\sin(\theta_0) = \pm\frac{2\pi n_{\text{eff}}}{\lambda_{\text{las}}} \pm m\frac{2\pi}{\Lambda} \quad (2)$$

where θ_0 is the angle of the mth diffracted order with respect to the normal. Substituting eqn (1) into eqn (2), we have $\theta_0 = 0°$. This means that there were two lasing output beams of equal intensities from one sample, and each beam was emitted in the direction perpendicular to the glass substrate. Fig. 7a shows the spectrum at a pump energy of 2× threshold. The single sharp peak with a bandwidth of 0.5 nm locates at 630.4 nm, and the emitted lasing output beams are totally TE polarized. Fig. 7b shows the dependence of output lasing intensity on the pumping energy. The threshold is indicated by a sudden increase in the slope, which is 0.18 μJ (0.036 mJ cm^{-2} or 4.5 kW cm^{-2}). The conversion efficiency of the pump input to the lasing output of the sample is 6.4%. Compared with the DFB laser (grating period at 590 nm) with a threshold of 0.68 μJ (0.136 mJ cm^{-2} or 17.0 kW cm^{-2}) and a conversion efficiency of 1.9%,[15] a dramatic enhancement of the lasing performance was achieved in this work. This result can be understood due to the following effects. One is from the second Bragg order used for the sample because the lower Bragg order can reduce the threshold effectively. This result further confirms the ability of the HPDLC technique in providing narrow gratings for second-order DFB lasers. The other reason is that the phase-separated LCs are aligned along the grating groove direction. The refractive index difference was measured to be 0.0195 in the sample, whereas the refractive index difference is 0.0054 in the sample at 590 nm as the phase separated LCs are aligned along the grating vector direction. The larger the refractive index, the better the lasing feedback performance. The refractive index difference can be deduced by Kogelnik's isotropic coupled wave theory.[24]

4. Conclusion

In conclusion, we have fabricated and characterized the second-order DFB laser based on a small period HPDLC grating. The optimum curing intensity, the orientation of LC molecules in HPDLCs with different grating periods and the lasing output were investigated. The results indicate that the anchoring energy of grating grooves would become stronger as the grating period decreases, and it is dominant in samples with narrower gratings, making LC molecules align along the grating groove direction. In this way, we greatly lowered the lasing output threshold and increased the conversion efficiency with no extra rubbing steps. We think this approach for the realization of effective microstructures is extremely competitive.

Conflicts of interest

There are no conflicts to declare.

Acknowledgements

The authors would like to thank the support from the high-level introduction of a talent research start-up fund and an experimental technology research project fund of Qufu Normal University (SJ201723).

References

1 T. Woggon, S. Klinkhammer and U. Lemmer, *Appl. Phys. B: Lasers Opt.*, 2010, **99**, 47–51.
2 Y. Yang, G. A. Turnbull and I. D. W. Samuel, *Adv. Funct. Mater.*, 2010, **20**, 2093–2097.
3 J. Clark and G. Lanzani, *Nat. Photonics*, 2010, **4**, 438–446.
4 Y. Yang, G. A. Turnbull and I. D. W. Samuel, *Appl. Phys. Lett.*, 2008, **92**, 163306.
5 (*a*) T. Riedl, T. Rabe, H.-H. Johannes, W. Kowalsky, J. Wang, T. Weimann, P. Hinze, B. Nehls, T. Farrell and U. Scherf, *Appl. Phys. Lett.*, 2006, **88**, 241116; (*b*) C. Karnutsch, M. Stroisch, M. Punke, U. Lemmer, J. Wang and T. Weimann, *IEEE Photonics Technol. Lett.*, 2007, **19**, 741–743.
6 S. Klinkhammer, X. Liu, K. Huska, Y. Shen, S. Vanderheiden, S. Valouch, C. Vannahme, S. Bräse, T. Mappes and U. Lemmer, *Opt. Express*, 2012, **20**, 3657–6364.

7 R. Xia, G. Heliotis and P. N. Stavrinou, *Appl. Phys. Lett.*, 2005, **87**(3), 031104.
8 B. Wenger, N. Tétreault, M. E. Welland and R. H. Friend, *Appl. Phys. Lett.*, 2010, **97**, 193303.
9 Y. Chen, J. Herrnsdorf, B. Guilhabert, A. L. Kanibolotsky, A. R. Mackintosh, Y. Wang, R. A. Pethrick, E. Gu, G. A. Turnbull, P. J. Skabara, I. D. W. Samuel, N. Laurand and M. D. Dawson, *Org. Electron.*, 2011, **12**, 62–69.
10 T. Zhai, X. Zhang, Z. Pang and F. Dou, *Adv. Mater.*, 2011, **23**, 1860–1864.
11 (*a*) T. J. Bunning, L. V. Natarajan, V. P. Tondiglia and R. L. Sutherland, *Annu. Rev. Mater. Sci.*, 2000, **30**, 83–115; (*b*) R. L. Sutherland, V. P. Tondiglia, L. V. Natarajan, T. J. Bunning and W. W. Adams, *Appl. Phys. Lett.*, 1994, **64**, 1074–1076; (*c*) C. Y. Li, M. J. Birnkrant, L. V. Natarajan, V. P. Tondiglia, P. F. Lloyd, R. L. Sutherland and T. J. Bunning, *Soft Matter*, 2005, **1**, 238–242; (*d*) Y. J. Liu, Y.-C. Su, Y.-J. Hsu and V. K. Hsiao, *J. Mater. Chem.*, 2012, **22**, 14191–14195; (*e*) Y. J. Liu, H. T. Dai and X. W. Sun, *J. Mater. Chem.*, 2011, **21**, 2982–2986; (*f*) L. Liu, W. Huang, Z. Diao, Z. Peng, Q.q. Mu, Y. Liu, C. Yang, L. Hu and L. Xuan, *Liq. Cryst.*, 2013, **41**, 145–152.
12 W. Huang, Y. Liu, Z. Diao, C. Yang, L. Yao, J. Ma and L. Xuan, *Appl. Opt.*, 2012, **51**, 4013.
13 Z. Diao, L. Kong, L. Xuan and J. Ma, *Org. Electron.*, 2015, **27**, 101–106.
14 I. Drevenšek-Olenik, M. Fally and M. A. Ellabban, *Phys. Rev. E: Stat., Nonlinear, Soft Matter Phys.*, 2006, **74**, 021707.
15 (*a*) L. Liu, L. Xuan, G. Zhang, M. Liu, L. Hu, Y. Liu and J. Ma, *J. Mater. Chem. C*, 2015, **3**(21), 5566–5572; (*b*) L. Liu, G. Zhang, X. Kong, Y. Liu and L. Xuan, *J. Phys. D: Appl. Phys.*, 2018, **51**(4), 045103.
16 G. Zhang, Q. Wang, Y. Liu, J. Ma, Z. Peng, L. Yao, D. Li, C. Yang, Q. Mu, Z. Cao and L. Xuan, *Org. Electron.*, 2017, **43**, 148–155.
17 W. Huang, Z. Diao, Y. Liu, Z. Peng, C. Yang, J. Ma and L. Xuan, *Org. Electron.*, 2012, **13**, 2307–2311.
18 W. Huang, Y. Liu, L. Hu, Q. Mu, Z. Peng, C. Yang and L. Xuan, *Org. Electron.*, 2013, 2299–2305.
19 W. Huang, D. Pu, S. Shen, G. Wei, L. Xuan and L. Chen, *J. Phys. D: Appl. Phys.*, 2015, **48**(37), 375303.
20 S. M. Guo, X. Liang, C. H. Zhang, M. Chen, C. Shen, L. Y. Zhang, X. Yuan, B. F. He and H. Yang, *ACS Appl. Mater. Interfaces*, 2017, **9**(3), 2942–2947.
21 F. Vita, D. E. Lucchetta, R. Castagna, L. Criante and F. Simoni, *J. Opt. A: Pure Appl. Opt.*, 2009, **11**, 024021.
22 R. Caputo, A. V. Sukhov, N. V. Tabirian, C. Umeton and R. F. Ushakov, *Chem. Phys.*, 2001, **271**, 323–335.
23 K. K. Vardanyan, J. Qi, J. N. Eakin, M. D. Sarkar and G. P. Crawford, *Appl. Phys. Lett.*, 2002, **81**, 4736–4738.
24 H. Kogelnik and C. V. Shank, *J. Appl. Phys.*, 1972, **43**, 2327–2335.

